


RESEARCH ARTICLE

The gas bladder of *Heterotis niloticus* (Cuvier, 1829)José M. Icardo¹  | Alessio Alesci² | Michal Kuciel³ | Krystyna Zuwała⁴ |
Maria C. Guerrero⁵ | Giacomo Zaccane⁶¹Department of Anatomy and Cell Biology,
Faculty of Medicine, University of Cantabria,
Santander, Spain²Department of Chemical, Biological,
Pharmaceutical and Environmental Sciences,
University of Messina, Messina, Italy³Poison Information Centre, Jagiellonian
University Medical College, Cracow, Poland⁴Department of Comparative Anatomy,
Faculty of Biology, Institute of Zoology and
Biomedical Research, Jagiellonian University,
Cracow, Poland⁵Department of Veterinary Sciences, Polo
Universitario dell'Annunziata, University of
Messina, Messina, Italy⁶Department of Biomedical and Dental
Sciences and Morphofunctional Imaging, Polo
Universitario dell'Annunziata, University of
Messina, Messina, Italy

Correspondence

José M. Icardo, Departamento de Anatomía y
Biología Celular, Facultad de Medicina, c/
Cardenal Herrera Oria, s/n, Santander 39011,
Spain.Email: icardojm@unican.es and
jose.icardo@unican.es

Abstract

This work reports on the structural characteristics of the respiratory gas bladder of the osteoglossiform fish *Heterotis niloticus*. The bladder-vertebrae relationships are also analyzed. A slit-shaped orifice in the mediodorsal pharyngeal wall is surrounded by a muscle sphincter and serves as a glottis-like opening to the gas bladder. The dorsolateral internal surface of the gas bladder is lined by a parenchyma of highly vascularized trabeculae and septa displaying an alveolar-like structure. The trabeculae contain, in addition to vessels, numerous eosinophils probably involved in immune responses. The air spaces are endowed with a thin exchange barrier indicating a good potential for respiratory gas exchange. The ventral wall of the gas bladder is a well-vascularized membrane that exhibits an exchange barrier in the luminal face and an inner structure dominated by the presence of a layer of richly innervated smooth muscle. This is suggestive of an autonomous adjustability of the gas bladder ventral wall. The trunk vertebrae show large transverse processes (parapophyses) and numerous surface openings that lead into intravertebral spaces that become invaded by the bladder parenchyma. Curiously, the caudal vertebrae show a regular teleost morphology with neural and hemal arches, but have similar surface openings and intravertebral pneumatic spaces. The African Arowana hence rivals the freshwater butterfly fish *Pantodon* in its exceptional role of displaying postcranial skeletal pneumaticity outside of Archosauria. The possible significance of these findings is discussed.

KEYWORDS

air-blood barrier, eosinophils, gas bladder, *Heterotis*, vertebrae, vertebral pneumaticity

1 | INTRODUCTION

Heterotis niloticus, also known as the African arowana, is a member of the Osteoglossiformes (bony-tongue fish), an early offshoot within teleosts. *Heterotis niloticus* makes aquatic gas exchange through gills and, after hatching, decreases the lamellar respiratory surface and becomes an obligate air breather using the gas bladder to make aerial gas exchange. The morphological changes implicated in gill atrophy have been described

recently (Zaccane et al., 2022) and are similar to those described for a representative of its sister genus, *Arapaima gigas* (Brauner et al., 2004; Gonzalez et al., 2010). In the two species, a large gas bladder becomes the main source of oxygen in the juvenile stages and thereafter (Fernandes et al., 2012; Graham, 1997).

Due to the close phylogenetic relationship between *Heterotis* and *Arapaima* (Hilton, 2003; Wilson & Murray, 2008), the morphological characteristics of the gas bladder have usually been described

This is an open access article under the terms of the Creative Commons Attribution License, which permits use, distribution and reproduction in any medium, provided the original work is properly cited.

© 2023 The Authors. *Journal of Morphology* published by Wiley Periodicals LLC.

together. In the two species, the gas bladder occupies the full length of the coelomic cavity and appears subdivided into a dorsolateral, spongy wall and a ventral, thin and compliant, richly vascularized wall (Dorn, 1968; Graham, 1997; Greenwood & Liem, 1984; Hyrtl, 1854; Liem, 1989). However, descriptions of the fine structure of the gas bladder have mostly been restricted to *Arapaima*. In this taxon, the gas bladder parenchyma consists of a network of trabeculae that delimit numerous air spaces or edicula of variable size. The trabeculae contain abundant blood vessels, are supported by smooth muscle and appear covered with respiratory epithelium formed by pavement and columnar cells (Fernandes et al., 2012; Scadeng et al., 2020). The respiratory surface exhibits the typical exchange barrier structure being formed by the capillary endothelium, the pavement cell cytoplasm and the basal lamina in between (Fernandes et al., 2012). Other structural details include the presence of abundant neutrophils in the blood vessels (Fernandes et al., 2012) and lymphoid infiltration of the trabeculae (Poll & Nysten, 1962). Most of these features appear to have been extrapolated to *Heterotis* without any in-depth examination. In addition, the structural characteristics of the gas bladder ventral wall have been neglected in the two species.

In other Osteoglossomorpha, the gas bladder maintains close relationships with the vertebrae. This is particularly the case in *Pantodon buchholzi*. The gas bladder of *Pantodon* shows gross morphological similarities with that of *Heterotis* and *Arapaima* (Graham, 1977; Greenwood & Liem, 1984; Liem, 1989). Early studies in *Pantodon* described the presence of a complex system of vertebral bone recesses that were invaded by the dorsolateral wall of the gas bladder, thus establishing respiratory spaces within the vertebral axis (Graham, 1997; Poll & Nysten, 1962). A recent study has brought about new information on the morphology of the *Pantodon* vertebrae and has found the gas bladder/bone interplay to be restricted to the large parapophyses (Icardo et al., 2020). The small size of this interplay makes it questionable to bear any significant role in terms of aerial respiration. However, epithelial invasion of the parapophyses remains as a distinctive feature of the *Pantodon* gas bladder. Although Osteoglossomorpha teleosts show the greatest diversity in gas bladder morphology (Liem, 1989), the possibility that the *Heterotis* gas bladder could have developed similar relationships with the vertebra has not been explored.

The morphology of the gas bladder of *H. niloticus* is described here. The gross morphology and fine structure of both the pharyngeal connection and the dorsolateral and ventral bladder walls have been studied. In addition, the relation between the gas bladder and the vertebrae has been analyzed. We report several undescribed structural features and the presence of pneumatic spaces in the vertebral centra that are invaded by respiratory tissue. The possible significance of all these findings is discussed.

2 | MATERIALS AND METHODS

Three adult specimens of *H. niloticus* (29–30 cm TL) were acquired from a local supplier and transferred to the laboratory where they were maintained in dechlorinated water at 26°C on a 14/10 h light/

dark cycle. Fish were killed by overdose with immersion in MS-222 (ethyl 3-aminobenzoate methanesulfonate; Sigma-Aldrich). Then, the ventral body wall was opened, part of the abdominal viscera removed and the fish were immersed in 3% glutaraldehyde in phosphate-buffered saline for fixation. In addition, the fixative was introduced into the gas bladder cavity by manual injection. All animal procedures were in agreement with the Declaration of Helsinki and with the Guide for the Care and Use of Laboratory Animals. Protocols for all experimental procedures were approved by the local Ethics Committee.

The fish were subjected to further dissection to expose the glottal area and the ventral and dorsolateral walls of the bladder. The dissections were photographed with an Olympus digital 800 camera (Olympus Imaging Corp.).

2.1 | Scanning electron microscopy (SEM)

Selected samples from the glottal area and the gas bladder dorsolateral and ventral walls were dehydrated in a series of graded acetone, dried by the critical point method and sputter coated with gold, following routine procedures. Samples were observed with an Inspect S microscope (FEI Company) working at 15–20 KV.

Additionally, spine fragments were subjected to maceration in 2N-NaOH for 7 days at room temperature and, then, in distilled water for another 2–3 days (Ohtani, 1987). This procedure was repeated several times until complete elimination of the soft tissues. Then, the isolated vertebrae were dehydrated in graded acetone, air-dried, and photographed with a binocular microscope or observed under the SEM microscope.

2.2 | Semi-thin sections and transmission electron microscopy (TEM)

Small tissue samples were postfixed in 1% osmium tetroxide, dehydrated in graded acetone and embedded in Araldite (Fluka, Buchs), following routine procedures. Semithin sections were cut with an LKB III ultratome, stained with 1% toluidine blue and observed with a Zeiss Axioskop 2 plus microscope equipped with an AxioCam HRC digital camera. For TEM, ultrathin sections cut with a Leica ultracut UCT were stained with uranyl acetate and lead citrate and examined with a Jeol-JEM-1011 working at 80 KV and equipped with a Gatan ORISUS SC 1000 CCD camera.

3 | RESULTS

3.1 | The gas bladder

The gas bladder of *H. niloticus* occupied the entire length of the coelomic cavity (Figure 1a). Its dorsolateral wall reached the lateral walls of the body cavity, and its membranous ventral wall faced the

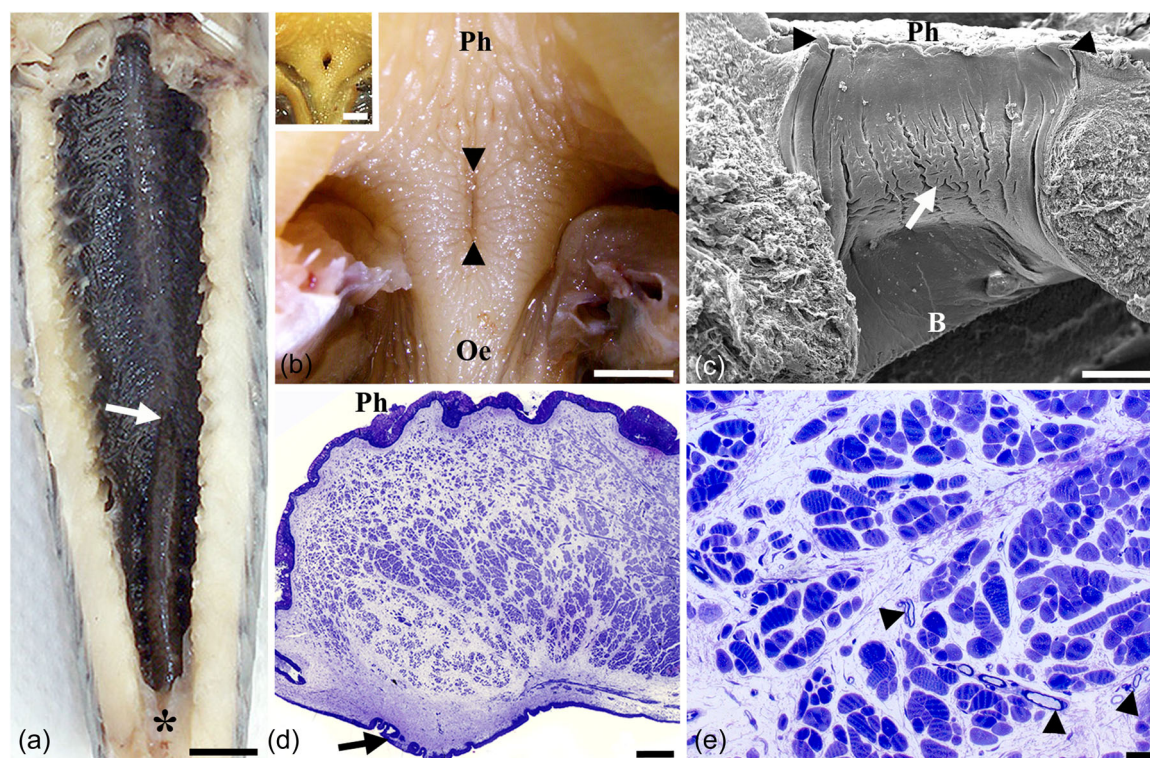


FIGURE 1 *Heterotis niloticus* bladder. (a) Ventral view. The body wall has been dissected to the boundary between the ventral and dorsolateral bladder walls. The visceral elements and the ventral wall, except the most caudal portion (asterisk), have been removed. The dorsolateral bladder wall occupies the coelomic cavity. The kidney appears as a longitudinal ridge that extends through the caudal third of the bladder (arrow). (b) Ventral view. The bladder opening is a dorsal, longitudinal slit (arrowheads) situated at the boundary between the pharynx (Ph) and the oesophagus (Oe). Inset of (b): The bladder opening is highlighted when the pharyngeal wall is pulled apart. (c) Scanning electron microscope (SEM). Left side of the pharyngeal connection. The limits of the glottal opening are indicated by arrowheads. The pharyngeal (Ph) epithelium is on top. A prominent ring (arrow) covered by an irregular epithelium encircles the glottal opening. The pharyngeal connection shows a smooth surface above and below the ring. B, bladder. (d) Semithin, transverse section of the pharyngeal connection. The ring (arrow) is formed by dense connective tissue. The pharyngeal connection contains numerous muscle bundles embedded in a loose matrix. Note the thickness of the Ph epithelium. (e) Semithin section. Skeletal muscle bundles are separated by a collagenous matrix rich in small vessels and nerve fibers (arrowheads). Magnification bars: (a) 1 cm; (b) 3 mm; inset of (b) 0.5 mm; (c) 0.5 mm; (d) 200 μ m; (e) 20 μ m.

remaining abdominal viscera. The bladder dorsolateral wall covered the kidney that appeared as a median ridge that tapered about the caudal third of the bladder length (Figure 1a).

The opening of the bladder was a midline slit located dorsally, at the boundary between the pharynx and the oesophagus (Figure 1b). The opening was short and was clearly highlighted only when the pharynx was pulled laterally (inset of Figure 1b). Dissection of this glottal-like opening revealed the presence of an inner, prominent ring covered by an epithelium marked by the presence of deep folds (Figure 1c). The presence of these folds contrasted with the smooth appearance of the rest of the glottal area. Histological examination showed that the ring was formed by a subepithelial accumulation of dense connective tissue (Figure 1d). In addition, the pharyngeal connection contained a muscular sphincter formed by loosely organized bundles of muscle (Figure 1d). The muscle exhibited the typical striated pattern and contained vessels of small caliber and abundant nerve fibers (Figure 1e). The rest of the connective tissue contained fibroblasts, collagen bundles and elastin fibers (not shown). No elongated or tube-like structure that could be referred to as a

pneumatic duct was present, the dorsal pharynx directly opening into the gas bladder via the aforementioned glottis-like structure (Figure 1c).

The luminal surface of the dorsolateral wall of the gas bladder showed interconnected trabeculae that appeared oriented roughly in a transverse direction. The trabeculae gave access to numerous air compartments of variable size that extended deeply into the parenchyma (Figure 2a). Using SEM, the surface trabeculae appeared as smooth bands whose borders extended deep to continue with the trabeculae delimiting the air spaces (Figure 2b). These surface bands were formed by dense connective tissue that usually carried vascular elements underneath (inset of Figure 2b).

The parenchyma was a spongy tissue formed by trabeculae of different sizes and thin septa (Figure 2c). Thick trabeculae contained, in addition to exchange capillaries, numerous blood vessels that occupied a large portion of the trabecular thickness (Figure 2d). Thin trabeculae could contain a single vessel making up for most of the wall thickness while the thinnest septa were often reduced to a central capillary covered by the respiratory epithelium (Figure 2d).

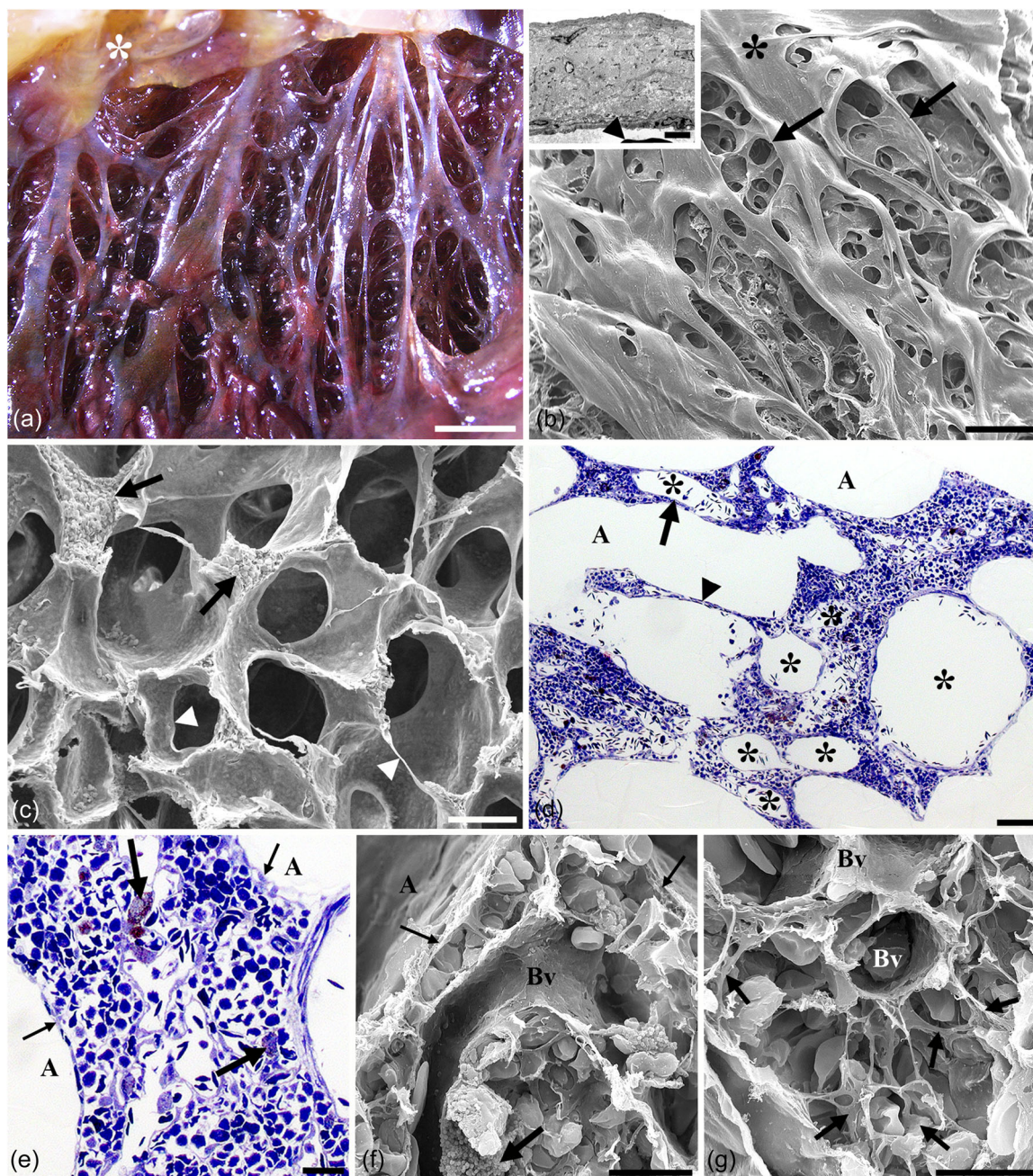


FIGURE 2 *Heterotis niloticus*, bladder dorsolateral wall. (a) Luminal surface. Interconnected trabeculae extend across the bladder width and give access to the air spaces. Asterisk, bladder ventral wall. (b) Scanning electron microscope (SEM). The trabeculae appear as surface bands continuous with the bladder ventral wall (asterisk). Arrows indicate continuity between the bands and the walls of the air spaces. Inset of (b): TEM. The surface bands are mostly formed by densely packed collagen. Arrowhead, erythrocyte in subjacent vessel. (c) SEM. Detail of the parenchyma. The air spaces are limited by trabeculae (arrows) and very thin septa (arrowheads). (d) Semithin section. Thick trabeculae contain large blood vessels (asterisks). Blood vessels could occupy most of the trabecular diameter (arrow). Thin septa (arrowhead) are reduced to the exchange capillary and the epithelial covering. A, air spaces. (e) Semithin section. A large capillary occupies the trabecular core. Numerous cells, including melanocytes (arrows), fill the space between the blood vessels. Exchange capillaries (thin arrows) face the air spaces (A). (f) SEM. Trabecular detail. A very thin boundary separates the central blood vessel (Bv) from the exchange capillaries (thin arrows) facing the air spaces (A). Numerous cells appear in the trabecular core. Arrow indicates a melanocyte with the cytoplasm filled with small granules. (g) SEM. The trabecular core shows numerous interstitial cells that extend cytoplasmic projections running among other structural elements including the wall of blood vessels (Bv). Magnification bars: (a) 2 mm; (b) 0.5 mm; inset of (b) 2 μ m; (c) 100 μ m; (d) 50 μ m; (e) 20 μ m; (f) 10 μ m; (g) 10 μ m.

Thick trabeculae also contained variable amounts of cellular elements (Figure 2e,f) that, with the exception of several melanocytes, could not be identified using the light microscope. Melanocytes appeared as large cells with a cytoplasm filled with numerous small granules (Figure 2e). The granular cytoplasm could also be identified by SEM (Figure 2f). Within the trabecular tissue, SEM also revealed the presence of interstitial cells showing stellated shapes and cytoplasmic prolongations that crossed the intercellular spaces connecting the different tissue components including blood vessels (Figure 2g).

Transmission electron microscopy demonstrated the presence in the trabecular core of eosinophil leukocytes, interstitial cells, extravasated erythrocytes, melanocytes, and occasional macrophages (Figure 3). Eosinophils constituted the main cell population and were characterized by the presence of numerous cytoplasmic granules (Figure 3a). The granules were rounded, showed moderate electron density and contained dark crystalline inclusions that could be surrounded by a clear halo (Figure 3b). In other cases, the centre of the granules could appear empty. Eosinophils were also observed in the blood and could be seen traversing the vessel wall (Figure 3b,

inset). Interstitial cells exhibited clear cytoplasm and were seen extending cytoplasmic prolongations among other cells (Figure 3a). Melanocytes could appear single or in small groups and were characterized by the presence of numerous, dense cytoplasmic granules (Figure 3c). Large macrophages were scattered through the trabeculae and contained numerous phagosomes and secondary lysosomes (Figure 3d). Neuroendocrine cells characterized by the presence of numerous, small, membrane-bound cytoplasmic granules were rare (not shown).

The surface of the air spaces was mostly covered by flattened, polygonal epithelial cells that showed a few small microvilli mostly distributed at the areas of cell confluence (Figure 4a). The thinness of the cytoplasm allowed to observe the casts of the underlying erythrocytes (Figure 4a,b). Additionally, a short number of epithelial cells showed reduced surface area and numerous, often irregular microvilli (Figure 4b,c and inset of c). These cells also showed thicker cytoplasm and cell overlapping (Figure 4c). The cell nucleus was located at these areas and its presence coincided often with the presence of the endothelial cell nucleus (Figure 4c and inset of c). The

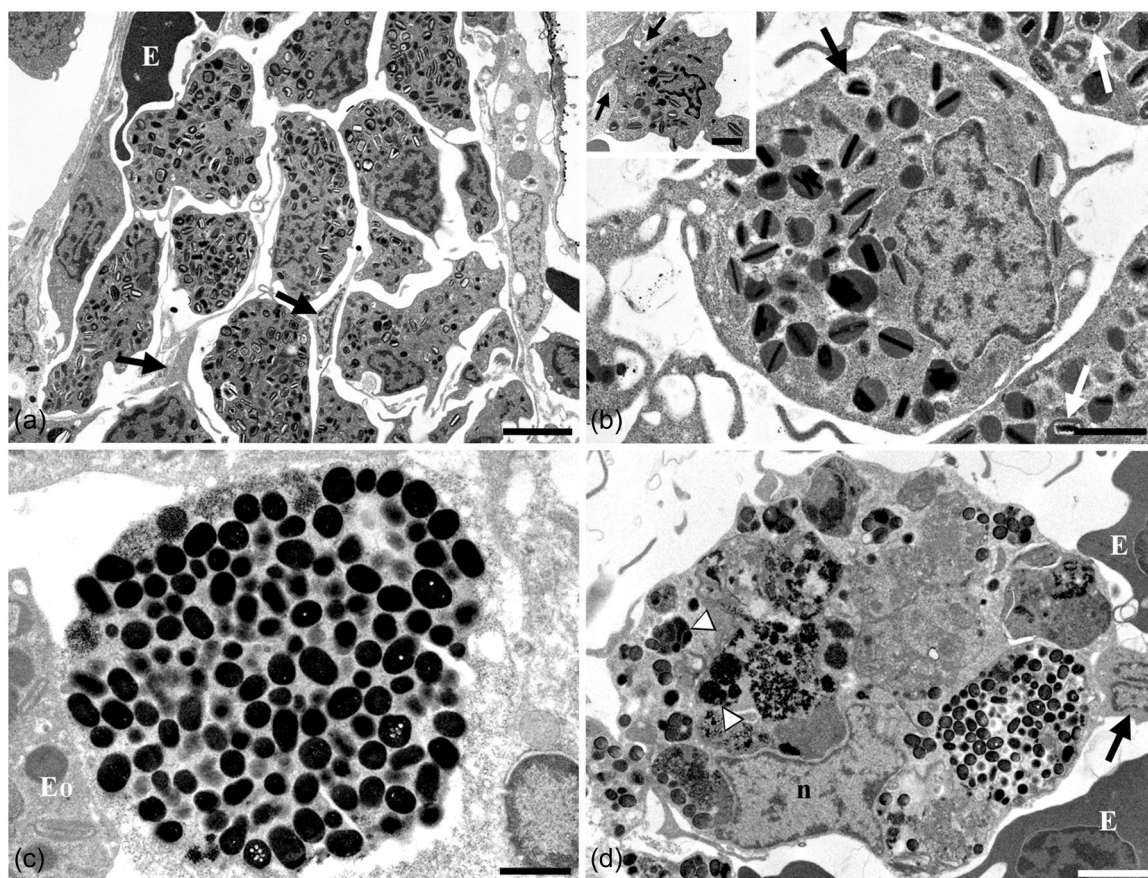


FIGURE 3 *Heterotis niloticus*, bladder dorsolateral wall. Transmission electron microscopy (TEM) of cellular components. (a) Most trabecular cells are eosinophil leukocytes. Arrows indicate interstitial cells extending thin prolongations among other cells. E, extravasated erythrocyte. (b) Eosinophil. Rounded cytoplasmic granules of moderate density show very dense crystallin inclusions. These inclusions may appear surrounded by a clear halo (arrow). Inset: An eosinophil is traversing the endothelial lining (arrows). Most of the cell body is in the vascular lumen. (c) Detail of a melanocyte. Very dense, small-size rounded granules pack the cell cytoplasm. Eo, eosinophil. (d) A large macrophage (n, nucleus) contains numerous bodies including secondary lysosomes (arrowheads). E, erythrocytes. Arrow, interstitial cell. Magnification bars: (a) 3 µm; (b) 1 µm; inset of (b) 1 µm; (c) 1 µm; (d) 2 µm.

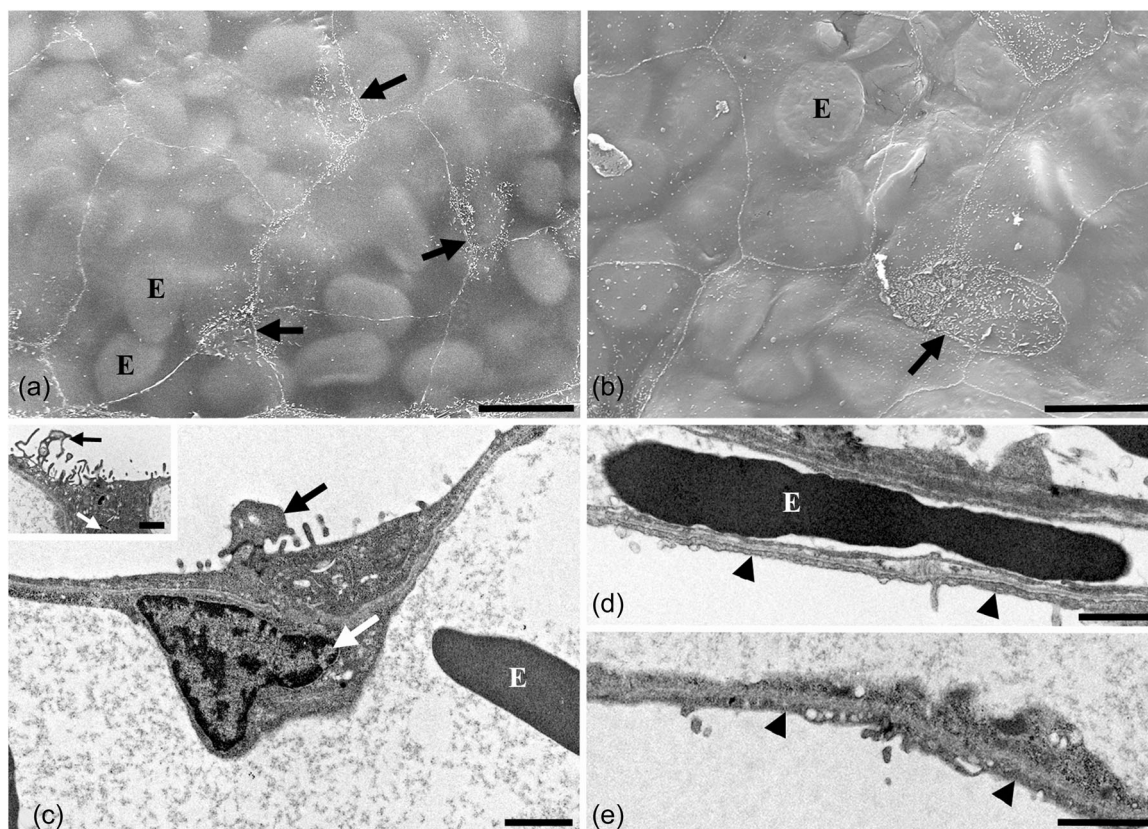


FIGURE 4 *Heterotis niloticus*, respiratory surface. (a) Scanning electron microscope (SEM). Flat, polygonal epithelial cells show microvilli at areas of cell confluence (arrows). E, underlying erythrocytes. (b) SEM. A few cells show reduced surface area and numerous microvilli (arrow). E, underlying erythrocytes. (c) Transmission electron microscopy (TEM). Cells with numerous microvilli show thick cytoplasm and cell overlapping (black arrow). White arrow indicates subjacent endothelial cell nucleus. E, erythrocyte. Inset of (c): Detail of irregular microvilli (black arrow). White arrow indicates the cell nucleus. (d) TEM. The epithelium (arrowheads) is separated from the capillary wall (E, erythrocyte) by a basement membrane with dense and lucent layers. (e) TEM. The interstitium between the epithelium (arrowheads) and the capillary wall is reduced to the dense layer. Magnification bars: (a) 10 µm; (b) 10 µm; (c) 1 µm; inset of (c) 1 µm; (d) 1 µm; (e) 1 µm.

number of these cells and the irregular microvilli appeared to increase near the luminal surface of the gas bladder. The air-blood barrier contained a thin layer of moderately dense basement membrane-like material flanked by lucent layers (Figure 4d). At many positions, the exchange barrier was reduced to the two cellular components and the dense material (Figure 4e). Nonetheless, the interstitial space appeared thicker and more irregular, and could show some fibrillar collagen and cellular extensions, close to the luminal surface.

The ventral wall of the gas bladder was a compliant, highly vascularized membrane. The peritoneal side was endowed with a simple epithelium while the luminal side showed the characteristics of an exchange barrier (Figure 5a). A large part of the ventral wall thickness was occupied by muscle bundles organized into one or two layers. The rest of the ventral wall contained loose connective tissue, vessels and nerves (Figure 5a). At the luminal side, the exchange barrier could show a regular appearance or be thickened with interposition of collagen fibers and cell prolongations between the surface epithelium and the vascular endothelium (Figure 5b). The muscular layer was formed by smooth muscle cells roughly oriented in the lateral direction (Figure 5c) although cells in the opposite

direction were also observed. Numerous amyelinic nerve fibers were in close contact with the muscle cells (Figure 5c and inset of c). Using SEM, the peritoneal side of the ventral wall was covered by polygonal, flattened cells with small microvilli, mostly located at the cell borders (Figure 5d). This face of the ventral wall also contained numerous collagenous threads probably resulting from the rupture of attachments to the removed viscera (inset of Figure 5d). In contrast, the surface facing the gas bladder lumen was a cell mosaic formed of polygonal, flattened cells with a few microvilli and of cells with very irregular surfaces extensively decorated with microvilli and protruding membrane folds (Figure 5e and inset of e). The underlying erythrocytes could be distinguished under the flattened cells (Figure 5e).

3.2 | The gas bladder-vertebrae relationships

Removal of the gas bladder from the dorsal body wall resulted in bladder rupture with portions of the parenchyma being retained within the vertebral bodies and in association with large

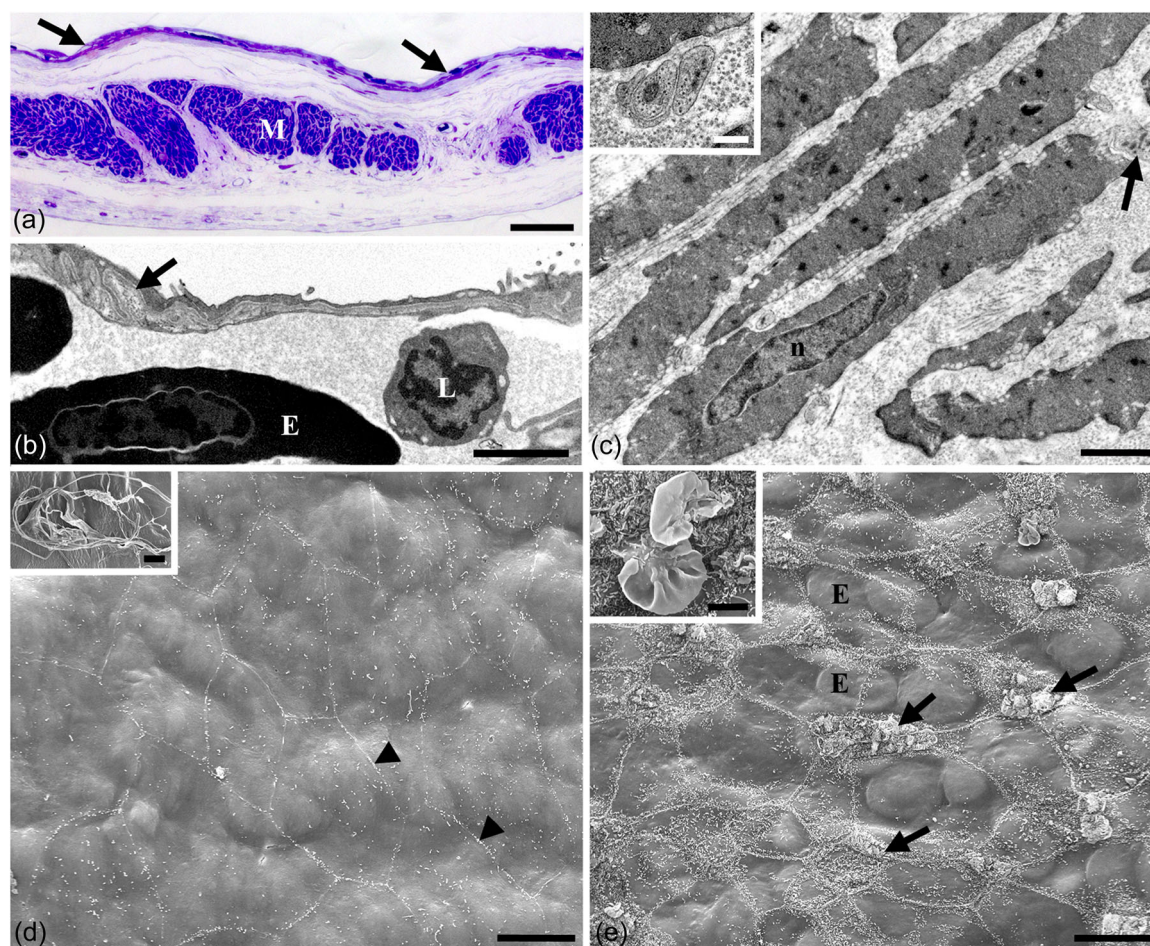


FIGURE 5 *Heterotis niloticus*, bladder ventral wall. (a) Semithin section. The luminal side shows an exchange barrier (arrows). Numerous muscle bundles (M) made up for a large portion of the wall. (b) Transmission electron microscopy (TEM). The exchange barrier shows regular areas and thickened segments (arrow) with accumulation of extracellular matrix and cell prolongations. Erythrocytes (E) and a lymphocyte (L) appear in the subjacent capillary. (c) TEM. Typical smooth muscle cells oriented in parallel form the muscle layer. n, nucleus. Arrow, nerve fiber. Inset of (c) Amyelinic axons surrounded by collagen are interposed between muscle cells. (d) Scanning electron microscope (SEM). Polygonal, flattened cells cover the peritoneal side. Arrowheads indicate cell border microvilli. Inset of (d): Collagen threads on the peritoneal side. (e): SEM. Luminal side. A mosaic of flattened and very irregular epithelial cells (arrows) covers this side of the ventral wall. E, erythrocytes under the flattened cells. Inset of (e): Detail showing numerous microvilli and two large membrane folds. Scale bars: (a), 30 μm ; (b), 2 μm ; (c), 1 μm ; inset of (c), 300 nm; (d), 10 μm ; inset of (d), 250 μm ; (e), 10 μm ; inset of (e), 3 μm .

parapophyses (Figure 6a). The presence of gas bladder tissue within the vertebral bodies was confirmed by SEM (Figure 6b). When the soft tissues were eliminated by NaOH digestion, isolated vertebra showed an hourglass autocentrum and two large parapophyses extending laterally (Figure 6c). The vertebral arcocentrum consisted of several craniocaudal ridges located along the body circumference. The ridges appeared in ventral, ventrolateral (Figure 6d,e) and in dorsal (Figure 6f,g) locations. The ridge located in the midventral position was always thicker and more complex, being often formed by the accretion of two or three ridges joined by short, transverse trabeculae (Figure 6d). The ridges delimited large openings in the vertebral surface that led into intravertebral pneumatic spaces. This occurred both at the ventrolateral (Figure 6d,e) and dorsal (Figure 6f,g) locations. Transverse sections of the vertebrae

(Figure 6h) confirmed the high degree of pneumatization of the vertebral bodies. These preparations also showed that the parapophyses arose from the vertebral body from several roots and that there was open communication between the base of the parapophyses and the intravertebral pneumatic spaces (Figure 6h).

To investigate the possible existence of morphological differences between the vertebrae at the trunk and caudal levels that could be related to the presence of the gas bladder, a segment of the tail immediately caudal to the anal opening was excised. Then, tail vertebrae were isolated and analyzed. Caudal vertebrae showed the typical neural and hemal arches oriented dorsoventrally (Figure 7a). In all the cases, craniocaudal ridges delimited in the lateral surfaces of the vertebral bodies one or two large orifices (Figure 7b), although the orifices could appear in more ventral and dorsal locations

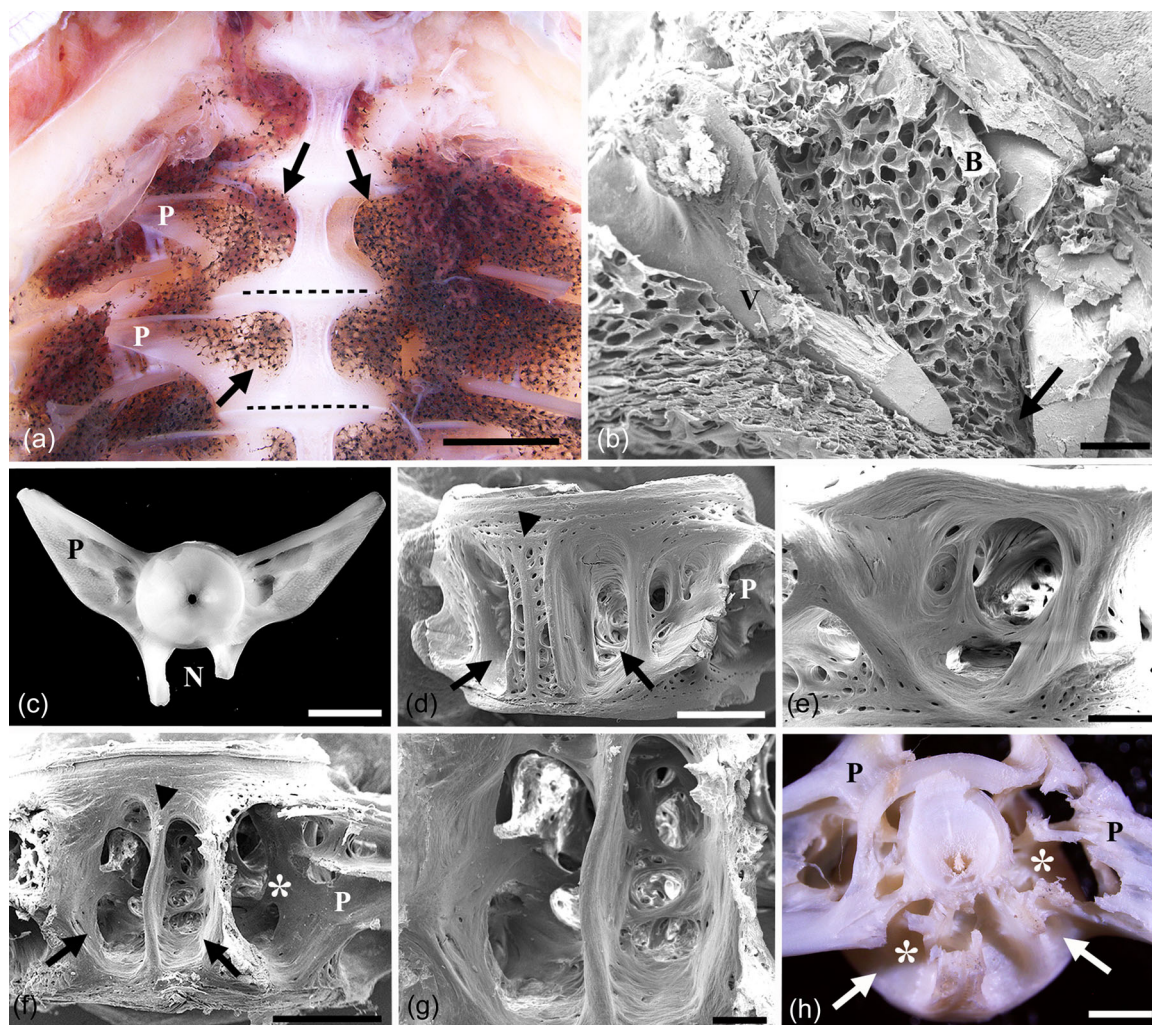


FIGURE 6 *Heterotis niloticus*, bladder-vertebrae relationship. (a) Binocular microscope. Removal of the bladder leaves bladder tissue within the vertebral body (arrows) and in association with large parapophyses (P). Broken lines indicate intervertebral discs. (b) Scanning electron microscope (SEM). Bladder tissue (B) appears within the vertebral body. V, ventral surface of vertebrae. Arrow indicates surface opening. (c) Binocular microscope. Cranial view of trunk vertebrae. Note hourglass shape, large parapophyses (P) and neural arch (N). (d) SEM. Ventrolateral view. Large surface openings (arrows) led into pneumatic spaces. Arrowhead indicates middorsal ridge. P, parapophysis. (e) SEM. Detail of surface opening and pneumatic spaces. Note trabecular reinforcement along the opening margins. (f) SEM. Dorsolateral view. Arrows indicate surface openings and pneumatic spaces. Arrowhead indicates middorsal ridge. Note continuity between the pneumatic space (asterisk) and the base of the parapophysis (P). (g) Detail of (f). Note dorsal ridges, surface openings, and pneumatic spaces. (h) Binocular microscope. Transverse section of vertebrae. Arrows indicate the openings leading into pneumatic spaces (asterisks). Note continuity between the base of the parapophyses (P) and the pneumatic spaces. Magnification bars: (a) 3 mm; (b) 5 mm; (c) 3 mm; (d) 1 mm; (e) 0,5 mm; (f) 1 mm; (g) 250 µm; (h) 1 mm.

(Figure 7c). Additional ventral and dorsal openings were also observed. In all the cases, the openings led into intravertebral pneumatic spaces (Figure 7b-d). The marginal borders of the surface openings were formed by compact tissue (Figure 7d). This contrasted with the appearance of the vertebral bodies that appeared formed by a meshwork of bony trabeculae, many of them keeping a dorsoventral orientation (Figure 7b,c). As it occurred at the trunk level, transverse sections of the vertebrae allowed to observe the spatial localization of both the ridges, surface openings, and pneumatic spaces (Figure 7e) (compare to Figure 6h).

4 | DISCUSSION

4.1 | The gas bladder

The absence of a pneumatic duct and the presence of a muscular sphincter in the pharyngeal connection coincide with early studies (Greenwood & Liem, 1984). The presence in the glottal opening of a prominent ring is intriguing. The ring has the structure of a connective pad that may provide for a better contact between opposing sides, therefore facilitating sealing of the pharyngeal connection.

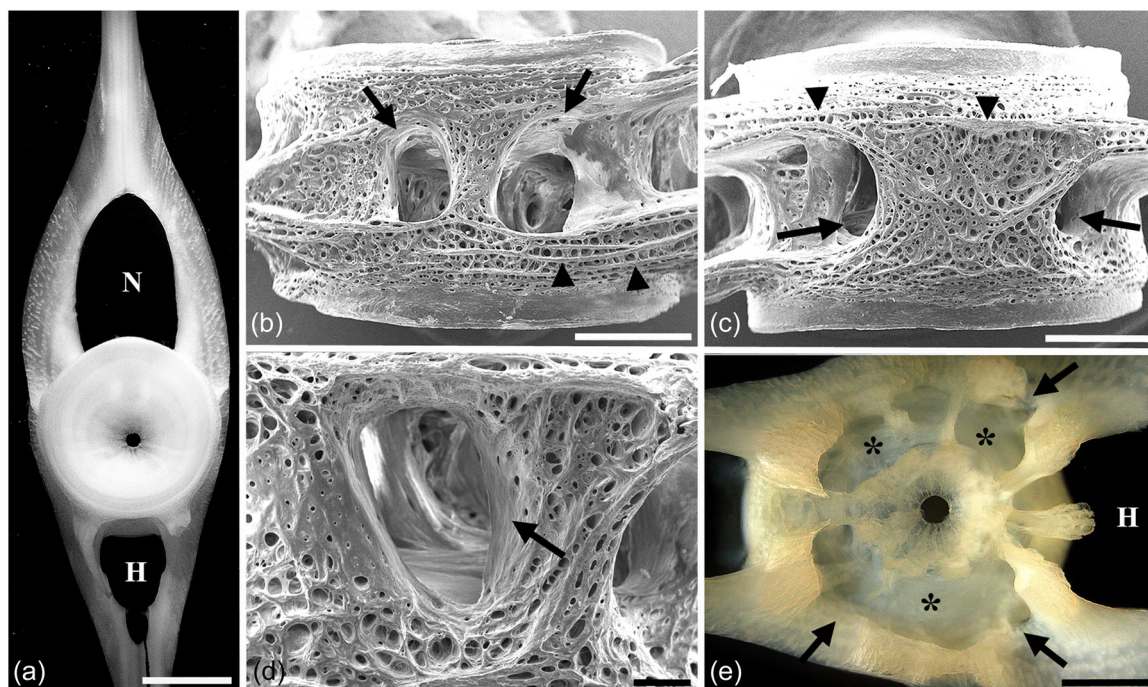


FIGURE 7 *Heterotis niloticus*, tail vertebrae. (a) Binocular microscope. Dorsal view. The vertebral body is located between the neural (N) and hemal (H) arches. (b) Scanning electron microscope (SEM). Lateral view: Two large orifices (arrows) led into pneumatic spaces. Arrowheads indicate dorsoventral bone trabeculae. (c) SEM: Lateral view. Two large orifices (arrows) appear in dorsolateral and ventrolateral locations. (d) SEM. Detail of surface orifice leading into pneumatic spaces. (e) Binocular microscope. Transverse section of vertebra. Arrows indicate the openings leading into the pneumatic spaces (asterisks). The central orifice communicates the two sides of the hourglass-shaped autocentrum. H, hemal arch. Magnification bars: (a) 2 mm; (b) 1 mm; (c) 1 mm; (d) 250 μ m; (e) 1 mm.

The parenchymal structure of the dorsolateral wall of the gas bladder coincides with previous observations (Greenwood & Liem, 1984; Poll & Nysten, 1962) and is in line with the structure of the gas bladder in related species such as *Pantodon* and *Arapaima* (see Graham, 1997). However, the absence of any bladder supporting structure like muscle or collagen that may serve as a structural scaffold is noteworthy. While collagen does not appear to be a relevant component of fish lungs and gas bladders, muscular components appear to play key supporting roles (Icardo, 2018). Skeletal and smooth muscle are present in the *Polypterus* lung (Icardo et al., 2017) and in the gas bladder of *Lepisosteus oculatus* (Icardo et al., 2015). However, only smooth muscle has been found in the lung of lungfish (Garofalo et al., 2015) and in the gas bladder of *Arapaima* (Fernandes et al., 2012; Scadeng et al., 2020). In *Pantodon*, the single representative of the Pantodontidae family of the Osteoglossomorpha, smooth muscle is also present in the gas bladder albeit in limited amounts (Icardo et al., 2020). In *Heterotis*, the interconnected superficial bands made of dense connective tissue constitute the single system able to provide structural support for the parenchyma. We suggest that these bands act as suspenders that, being extended across the bladder width, maintain the air spaces open by avoiding structural collapse. Probably, this system is effective only in the portions of the gas bladder closer to the lumen. When the bladder tissue attaches to the vertebral elements, bone attachment may be sufficient to maintain the air spaces open (see Fernandes et al., 2012).

Another curious feature is the bladder vascular richness. Although respiratory gas bladders usually contain numerous blood vessels (Icardo et al., 2015, 2020), a large portion of the gas bladder parenchyma is made up of vascular elements in *Heterotis*. The presence of a prominent vascular meshwork may contribute to support the bladder structure. A high vascular content is also present in the *Arapaima* gas bladder (Fernandes et al., 2012) and has been related to its respiratory role. The *Arapaima* gas bladder supplies about three quarters of all the animal oxygen needs (Brauner et al., 2004). Similar levels of oxygen uptake might be expected for the *Heterotis* gas bladder.

In addition to blood vessels, the thicker trabeculae of the gas bladder contain several cell types including interstitial cells and eosinophils. Interstitial cells extend elongated cell processes across the intercellular spaces that connect the trabecular components and appear to provide for structural support and tissue organization. Interstitial cells appear to play similar roles in the *Pantodon* gas bladder (Icardo et al., 2020). On the other hand, eosinophil leukocytes constitute a large cell population. Numerous eosinophils are also present in the *Pantodon* gas bladder and their presence has been related to the cell capability to develop immune responses against external pathogens (see Icardo et al., 2020). Indeed, eosinophils constitute a first line of defense in organs exposed to the external environment in vertebrates (Bloom & Fawcett, 1994). This general role could probably be extended to other respiratory gas bladders.

explaining eosinophil accumulation. Note that eosinophils accumulate in the absence of any signs of tissue infection and/or inflammation.

The epithelium covering the air spaces is mostly formed by polygonal cells with flattened cytoplasm and a few microvilli. The additional presence of epithelial cells showing columnar shape, reduced surface area and a high number of microvilli could be misinterpreted as proof of the existence of pneumocytes types 1 and 2. However, type-2 pneumocytes are characterized by the production, storage, and secretion of surfactant molecules stored in lamellar bodies (Bloom & Fawcett, 1994). The absence of lamellar bodies and of structural evidence of cellular secretion suggest the presence of a single pneumocyte type in the *Heterotis* gas bladder. The thickness of the cell cytoplasm and the reduction of the surface area may simply be due to the presence of the cell nucleus and to the concentration of cytoplasmic organelles. However, similar columnar cells have been shown to contain lamellar bodies in *Arapaima* (Fernandes et al., 2012). Whether this represents a species difference, a different functional status or even an artefactual problem, is presently unknown. Under the pavement epithelium, a thin basement membrane separates the pneumocytes from the capillary wall. The thinness of the exchange barrier, with the interstitial space often reduced to the dense layer of the basement membrane, suggests a high potential efficiency in gas exchange. Similar structural characteristics and high diffusing capacity have been reported in *Arapaima* (Fernandes et al., 2012). The thinness of the air-blood barrier explains SEM visualization of the underlying erythrocytes.

The ventral wall of the gas bladder shows two main morphological features. First, its luminal side shows the presence of an exchange barrier. This certainly increases the area of gas exchange. However, the fact that the barrier presents thinner and thicker areas indicates a poorer physiological performance than the barrier in the dorsolateral wall. This face of the ventral wall also lacks cells with lamellar bodies. It is curious that, in *Pantodon*, cells on the luminal side show lamellar bodies in the absence of a barrier exchange (Icardo et al., 2020). This probably indicates different physiological needs in closely related species. Another important feature is the presence of a well-developed smooth muscle layer. Smooth muscle cells and nerves are also present in the ventral wall of *Pantodon* (Icardo et al., 2020), but the higher structural organization and rich innervation are more similar to those observed in *Arapaima* (unpublished observations). Previous physiological studies suggested that the gas bladder ventral wall plays an important role during *Arapaima* ventilation (Farrell & Randall, 1978). Although there is some controversy on this point (Greenwood & Liem, 1984), our results provide structural support for an autonomous regulation during gas bladder ventilation.

4.2 | The gas bladder-vertebrae relationships

A main finding of this work is the presence of pneumatic spaces within the vertebral bodies. These spaces are occupied by the gas bladder respiratory tissue. To our knowledge, this is the first demonstration of postcranial skeletal pneumaticity of vertebral centra in a taxon other than

extant birds and extinct archosaurs (see O'Connor, 2006, 2009). The difference is that, in birds, the vertebral centra are invaded by epithelial protrusions of the air sacs, which itself bud out of the lungs as ventilatory structures (see Lambert et al., 2018; O'Connor, 2006). Pneumatization of vertebral elements has previously been reported in two other fish species but they are restricted to the transverse processes. In *Pantodon*, the large parapophyses are invaded by the respiratory bladder (Icardo et al., 2020; Poll & Nysten, 1962) while a non-respiratory swim bladder develops bulla inside the transverse processes of the deep-sea fish *Scombrobrax heterolepis* (Bond & Uyeno, 1981). In *Heterotis*, vertebral expansion of the gas bladder not only increases the respiratory area but may serve additional functions such as decreased density and buoyancy control. Our results indicate that vertebral pneumatization is not exclusive of living birds. It could come as no surprise if further studies find similar features in other fish species.

Another significant finding of this work is the presence of morphological differences between the vertebrae of the body and tail. While the trunk vertebrae show large lateral processes oriented transversely, caudal vertebrae show the typical teleost configuration with neural and hemal arches oriented dorsoventrally. These differences also occur in *Pantodon* and appear to be related to the presence of the respiratory gas bladder (Poll & Nysten, 1962). Noticeably, caudal vertebrae also exhibit surface foramina and pneumatic spaces despite the absence of respiratory tissue. It could then be inferred that vertebral pneumaticity and bladder invasion are independent features, the bladder invading pre-existing spaces at the trunk level. This inference would work for both birds and bird-like archosaurs (see Lambert et al., 2018). However, previous observations in *Heterotis* have reported on the presence of a saccular organ located between the hemal arches of the caudal vertebra. This organ appears to be filled with air and communicates cranially with the gas bladder (Poll & Nysten, 1962). The functional significance of this exceptional morphological arrangement, including a potential ventilatory role, warrants further examination.

ACKNOWLEDGMENTS

The authors wish to thank R. García-Ceballos and F. Madrazo (Instituto de Investigación Valdecilla -IDIVAL-) for technical assistance.

CONFLICT OF INTEREST STATEMENT

The authors declare no conflict of interest.

DATA AVAILABILITY STATEMENT

Data are available on request.

ORCID

José M. Icardo  <http://orcid.org/0000-0001-9543-2444>

PEER REVIEW STATEMENT

The peer review history for this article is available at <https://www.webofscience.com/api/gateway/wos/peer-review/10.1002/jmor.21584>.

REFERENCES

- Bloom, W., & Fawcett, D. W. (1994). *A textbook of histology* (12th ed.). Chapman & Hall.
- Bond, C. E., & Uyeno, T. (1981). Remarkable changes in the vertebrae of perciform fish *Scombrobrax* with notes on its anatomy and systematics. *Japanese Journal of Ichthyology*, 28, 259–262.
- Brauner, C. J., Matey, V., Wilson, J. M., Bernier, N. J., & Val, A. L. (2004). Transition in organ function during the evolution of air-breathing; insights from *Arapaima gigas*, an obligate air-breathing teleost from the Amazon. *Journal of Experimental Biology*, 207, 1433–1438.
- Dorn, E. (1968). Schwimmblasenbau und lebensweise der osteoglossiden. *Verhandlungen der Deutschen Zoologischen Gesellschaft*, 31, 370–380.
- Farrell, A. P., & Randall, D. J. (1978). Air-breathing mechanics in two Amazonian teleosts, *Arapaima gigas* and, *Hoplerthrinus unitaeniatus*. *Canadian Journal of Zoology*, 56, 939–945.
- Fernandes, M. N., da Cruz, A. L., da Costa, O. T. F., & Perry, S. F. (2012). Morphometric partitioning of the respiratory surface area and diffusion capacity of the gills and swim bladder in juvenile Amazonian air-breathing fish, *Arapaima gigas*. *Micron*, 43, 961–970.
- Gonzalez, R. J., Brauner, C. J., Wang, Y. X., Richards, J. G., Patrick, M. L., Xi, W., Matey, V., & Val, A. L. (2010). Impact of ontogenetic changes in branchial morphology on gill function in *Arapaima gigas*. *Physiological and Biochemical Zoology*, 83, 322–332.
- Graham, J. B. (1997). *Air-breathing fishes. Evolution, diversity and adaptation* (p. 299). Academic Press.
- Greenwood, P. H., & Liem, K. F. (1984). Aspiratory respiration in *Arapaima gigas* (Teleostei, Osteoglossomorpha): A reappraisal. *Journal of Zoology*, 203, 411–425.
- Hilton, E. J. (2003). Comparative osteology and phylogenetic systematics of fossil and living bony-tongue fishes (Actinopterygii, Teleostei, Osteoglossomorpha). *Zoological Journal of the Linnean Society*, 137, 1–100.
- Hyrtl, J. (1854). Beitrag zur Anatomie von *Heterotis ehrenbergii*. C. V. Wien *Denkschriften*, 8, 73–88.
- Icardo, J. M. (2018). Lungs and gas bladders: Morphological insights. *Acta Histochemica*, 120, 605–612.
- Icardo, J. M., Capillo, G., Lauriano, E. R., Kuciel, M., Aragona, M., Guerrero, M. C., & Zaccane, G. (2020). The gas bladder of *Pantodon buchholzi*: Structure and relationships with the vertebrae. *Journal of Morphology*, 281, 1588–1597.
- Icardo, J. M., Colvee, E., Kuciel, M., Lauriano, E. R., & Zaccane, G. (2017). The lungs of *Polypterus senegalus* and *Erpetoichthys calabaricus*: Insights into the structure and functional distribution of the pulmonary epithelial cells. *Journal of Morphology*, 278, 1321–1332.
- Icardo, J. M., Colvee, E., Lauriano, E. R., Capillo, G., Guerrero, M. C., & Zaccane, G. (2015). The structure of the gas bladder of the spotted gar, *Lepisosteus oculatus*. *Journal of Morphology*, 276, 90–101.
- Lambertz, M., Bertozzo, F., & Sander, P. M. (2018). Bone histological correlates for air sacs and their implications for understanding the origin of the dinosaurian respiratory system. *Biology Letters*, 14, 20170514.
- Liem, K. F. (1989). Respiratory gas bladders in teleosts: Functional conservatism and morphological diversity. *American Zoologist*, 29, 333–352.
- O'Connor, P. M. (2006). Postcranial pneumaticity: An evaluation of soft-tissue influences on the postcranial skeleton and the reconstruction of pulmonary anatomy in archosaurs. *Journal of Morphology*, 267, 1199–1226.
- O'Connor, P. M. (2009). Postcranial pneumaticity: Evolution of archosaurian body plans: Skeletal adaptations of an air-sac-based breathing apparatus in birds and other archosaurs. *Journal of Morphology*, 311A, 629–646.
- Ohtani, O. (1987). Three-dimensional organization of the connective tissue fibers of the human pancreas. A scanning electron microscopic study of NaOH treated tissues. *Archivum Histologicum Japonicum*, 50, 557–566.
- Poll, M., & Nysten, M. (1962). Vessie natatoire pulmonaire et pneumatization des vertèbres chez *Pantodon buchholzi* Peters. *Bulletin des Séances*, 8, 434–454.
- Scadeng, M., McKenzie, C., He, W., Bartsch, H., Dubowitz, D. J., Stec, D., & St. Leger, J. (2020). Morphology of the Amazonian teleost genus *Arapaima* using advanced 3D imaging. *Frontiers in Physiology*, 11, 260.
- Wilson, M. V. H., & Murray, A. M. (2008). Osteoglossomorpha: Phylogeny, biogeography, and fossil record and the significance of key African and Chinese fossil taxa. *Geological Society, London, Special Publications*, 295, 185–219.
- Zaccane, G., Capillo, G., Aragona, M., Alesci, A., Cupello, C., Lauriano, E. R., Guerrero, M. C., Kuciel, M., Zuwala, K., Germana, A., & Icardo, J. M. (2022). Gill structure and neurochemical markers in the African bonytongue (*Heterotis niloticus*): A preliminary study. *Acta Histochemica*, 124, 151954.

How to cite this article: Icardo, J. M., Alesci, A., Kuciel, M., Zuwala, K., Guerrero, M. C., & Zaccane, G. (2023). The gas bladder of *Heterotis niloticus* (Cuvier, 1829). *Journal of Morphology*, 284, e21584.
<https://doi.org/10.1002/jmor.21584>